JOURNAL OF CATALYSIS 95, 396–405 (1985)

Surface Analysis of Methylchlorosilane Formation Catalysts

TIMOTHY C. FRANK, KEITH B. KESTER,[1] AND JOHN L. FALCONER[2]

Department of Chemical Engineering, University of Colorado, Campus Box 424, Boulder, Colorado 80309

Received December 19, 1984; revised April 30, 1985

The surfaces of Cu_3Si and Cu_3Si containing 0.4 at.% Zn (Cu_3Si–Zn) were analyzed with Auger spectroscopy, as a function of reaction temperature, before and after reaction with atmospheric-pressure CH_3Cl. These surfaces, which selectively form $(CH_3)_2SiCl_2$, contained silicon, copper, chlorine, carbon, and a small amount of oxygen after reaction. The Cu_3Si–Zn surface also contained zinc. The Si(LVV) Auger transition exhibited chemical shifts which indicated the presence of Si—Cl, Si—C, and Si—Cu bonds. Active sites for selective $(CH_3)_2SiCl_2$ formation appear to contain silicon bound to chlorine. Copper weakens silicon bonds in the alloy, and this may result in faster Si—Cl bond formation and shorter induction times than for the uncatalyzed reaction. Silicon carbide sites, which do not contain chloride, are also present after reaction, but apparently do not form silanes. The Cu_3Si and Cu_3Si–Zn surfaces differ dramatically after reaction. The fraction of surface silicon which formed silicon carbide sites was smaller for Cu_3Si–Zn than for Cu_3Si; however, the Cu_3Si–Zn surface contained up to 85% graphitic carbon though no graphite was detected on Cu_3Si. Zinc may promote conversion of carbide to graphitic carbon. Graphite did not significantly affect silane formation kinetics, however, suggesting that only a fraction of the surface was active for silane formation.

INTRODUCTION

Recently, we reported methylchlorosilane formation rates for the reaction of atmospheric-pressure methyl chloride with low-surface-area Cu_3Si alloys (*1*). Reaction on these alloy surfaces selectively forms dimethyldichlorosilane, a monomer used commercially to produce silicone polymers (*2*). In that study (*1*), the surfaces were cleaned in ultrahigh vacuum (UHV) and characterized with Auger electron spectroscopy (AES) before reaction. Reaction with CH_3Cl changed the surface composition significantly. The results of AES surface analysis immediately after reaction, without air exposure, are reported here for Cu_3Si and Cu_3Si containing zinc promoter. Surface compositions of reacted copper–silicon solids have not been measured previously without prior exposure of the surface to the atmosphere. This exposure rapidly oxidizes Cu_3Si (*3*) and thus significantly distorts measurement of the composition present during reaction conditions. Previous reaction studies have also used high-surface-area copper–silicon particles instead of low-surface-area samples that are easier to analyze.

Auger spectroscopy is well suited for studying the surfaces of copper–silicon alloys since copper and silicon Auger transitions do not overlap. Also, since the Si(LVV) transition is sensitive to the chemical environment, surface concentration estimates and information about bonds formed to silicon can be obtained.

Our reaction study (*1*) showed that Cu_3Si provides an active surface for selective $(CH_3)_2SiCl_2$ formation. Copper acts as a catalyst for this selective reaction (up to 85% of the silane products are $(CH_3)_2SiCl_2$); in the absence of copper less than 1% of the silane products are $(CH_3)_2SiCl_2$ (*4*). Zinc promoter is used in low concentrations to further increase selectivity (*1*).

EXPERIMENTAL METHODS

Auger spectra of Cu_3Si and Cu_3Si con-

[1] On leave from the Chemistry Department, Colorado College, Colorado Springs, Colo. 80903.

[2] To whom correspondence should be addressed.

0021-9517/85 $3.00

taining 0.4 at.% Zn were recorded before and after reaction with CH_3Cl at 84 kPa (635 Torr) and 520–620 K (*1*). A metal-bellows mechanism transferred the alloy samples between a differential batch reactor and a UHV chamber which contained a PHI Model 10-155 CMA for Auger analysis (*1, 3*). Surfaces were cleaned by argon ion bombardment using procedures described previously (*3*).

The Cu_3Si alloy contained 23 at.% Si and 77 at.% Cu, since precipitates form at higher silicon concentrations (*5*). The promoted alloy contained 22.1 at.% Si, 77.5 at.% Cu, and 0.4 at.% Zn (*6*). The Cu_3Si phase was verified for both alloys using polarized-light microscopy and X-ray diffraction (*3, 6*). The clean Cu_3Si alloy was also extensively characterized by Auger electron spectroscopy (*3*).

Each nonporous alloy sample (approx. 1 × 5 × 13 mm) was cleaned and annealed at 570 K for 15 min in UHV, characterized by AES, and then transferred into the reactor. The reactor was then pressurized with CH_3Cl to 84 kPa (635 Torr). The alloy sample was heated resistively and temperature was measured with a Chromel-Alumel thermocouple spotwelded to the alloy edge. Reaction gases were sampled with a Valco GC valve (0.5 cm^3 sampling volume) and analyzed by an HP 5712 GC with thermal conductivity detector. After reaction at constant temperature, the solid sample was cooled to 310 K, the reactor evacuated, and the sample transferred into the UHV chamber for AES analysis. Auger spectra were recorded within 5 min of evacuating the reactor. Alloy samples were recleaned and annealed before each isothermal run.

Several steps were taken to minimize impurity concentrations during reaction; the reactor system was leak-checked and baked at UHV pressures, the CH_3Cl gas (Matheson, 99.95% pure) was purified with 5-Å molecular sieve at 273 K to remove CH_3OH, and the region around the sampling valve was flushed with dry nitrogen to prevent leakage of air into the reactor during gas sampling.

Auger spectra were first recorded with a 2-keV, 5-μA primary beam to minimize desorption, and then with a 3-keV, 30-μA beam for higher sensitivity; all figures show 3-keV spectra. Surface concentrations were *estimated* using 3-keV spectra since peak shapes were the same for each beam energy and since handbook sensitivity factors are not available for a 2-keV beam. A 1-V p–p modulation was used for all peaks except Si(1620 eV), for which 6-V p–p was used. Details of the apparatus and experimental procedures are reported elsewhere (*1, 7*).

RESULTS

Auger Spectra

Following CH_3Cl reaction to form silanes on Cu_3Si and Cu_3Si–Zn (*1*), Auger analysis of these surfaces indicated the presence of

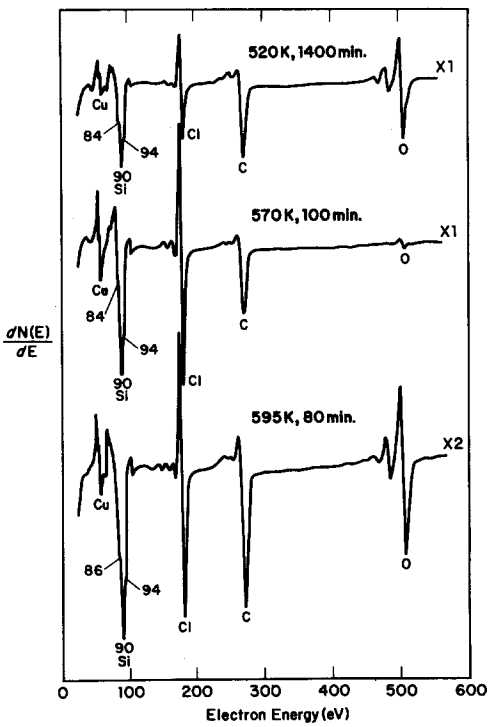

FIG. 1. Auger spectra of Cu_3Si after reaction with 84 kPa CH_3Cl at the indicated temperatures and times.

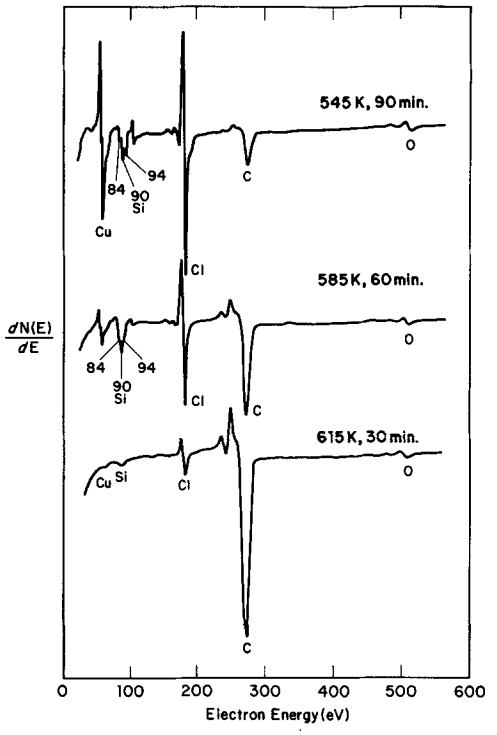

FIG. 2. Auger spectra of Cu_3Si–Zn after reaction with 84 kPa CH_3Cl at the indicated temperatures and times.

silicon, copper, chlorine, carbon, and oxygen. The Cu_3Si–Zn surface also contained zinc. Figures 1 and 2 show the Cu(60, 105 eV), Si(75–94 eV), Cl(180 eV), C(273 eV), and O(508 eV) Auger peaks for Cu_3Si and Cu_3Si–Zn. The Si(1620 eV) and Cu(917 eV) peaks, which had the same shapes as seen for clean Cu_3Si (*3*), were also recorded. The Zn(994 eV) peak, whose shape was not well resolved due to the low zinc concentration, had the same energy as elemental zinc (*8*). Peak shapes and locations in the spectra of clean Cu_3Si–Zn were similar to those for clean Cu_3Si (*3*), though the amplitudes differed.

During reaction with CH_3Cl, the silicon chemical environment at both alloy surfaces changed significantly, as indicated by the change from the split Si(90 and 94 eV) peaks seen for clean Cu_3Si alloys to a series of peaks at 75 to 94 eV (Fig. 3). These spectra apparently resulted from several silicon chemical states. Silicon bound to elements of greater electronegativity yields peaks which are shifted from 92 eV, the peak location for elemental silicon, to lower energies, and the peak shift increases with increasing electronegativity (*4, 9*). Thus, Si—C, Si—Cl, and Si—O bonds yield Si(LVV) peaks at 90, 84, and 76 eV, respectively (*4*). Since peak shift is approximately an exponential function of the electronegativity difference (Pauling scale) between silicon and the element bound to silicon (*4*), if silicon is bound to several elements, the most electronegative element will determine Si(LVV) peak location. Additional silicon bonds to elements of lower electronegativity cause little additional peak shift.

Surface concentrations (Tables 1 and 2) were *estimated* from Si(1620 eV), Cu(917 eV), Cl(180 eV), C(273 eV), O(510 eV), and Zn(994 eV) peak amplitudes and handbook sensitivity factors (*8*). Matrix-effect correction factors were not used since accurate factors are not available for nondilute, multicomponent surfaces (*9*). Although Si(LVV) electrons are more surface-sensi-

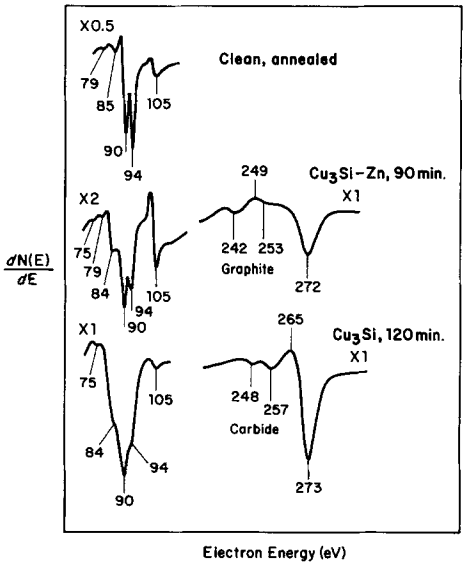

FIG. 3. Si(LVV), Cu(105 eV), and C(KVV) Auger peaks for Cu_3Si–Zn and Cu_3Si after reaction at 545 K for the indicated times. Spectra of clean, annealed (570 K) Cu_3Si are included for comparison.

TABLE 1

Estimated Cu_3Si Surface Concentrations

Surface	Temperature (K)	Concentration (atomic percent)					Silicon reacted (10^2 monolayers)	Reaction time (min)
		Si	Cu	Cl	C[a]	O		
Ion bombarded	—	25	75	0	0	0	0	0
Clean, annealed	570	30	70	<1	0	0	0	0
After reaction	520	33	38	4	19	6	4.4	1400
	545	31	38	8	18	5	4.6	120
	570	27	50	10	13	<1	<0.3	5
	570	30	44	10	16	<1	5.3	100
	595	31	39	6	18	6	22	80

[a] Carbide.

tive than Si(1620 eV) electrons (0.5 versus 1.5 nm escape depth) (*9*), the Si(1620 eV) peak was used to estimate surface concentrations since the dramatic changes in shape and location of the Si(LVV) peak indicate that its amplitude was not proportional to concentration. The Cu(917 eV) peak, whose escape depth is close to that for Si(1620 eV) (*9*), was used so that surface composition estimates were not skewed by large differences in escape depth. Use of the more surface-sensitive Cu(60 eV) peak *reduced* the copper concentration estimates in Tables 1 and 2 by about 50%, indicating that the estimates of copper surface concentrations in these tables are high. The reproducibility of the concentration estimates for clean, annealed surfaces was ±2 percentage points. Though the values in Tables 1 and 2 are only estimates of surface compositions, they are useful for comparing the two surfaces and the same surface at different temperatures.

The C(KVV) peak shapes after reaction indicate that silicon carbide is present at Cu_3Si surfaces, but that graphitic carbon is present at Cu_3Si–Zn surfaces (Fig. 3) (*9*). Because the carbon peak shapes for the two

TABLE 2

Estimated Cu_3Si–Zn Surface Concentrations

Surface	Temperature (K)	Concentration (atomic percent)						Silicon reacted (10^2 monolayers)	Reaction time (min)
		Si	Cu	Cl	C[a]	O	Zn		
Ion bombarded	—	20	79	0	0	0	<1	0	0
Clean, annealed	570	27	71	<1	<1	0	2	0	0
After reaction	545	11	58	15	14	1	1	6.1	90
	570	11	46	15	26	1	1	8.2	90
	585	15	35	9	40	1	<1	15	60
	595	9	14	6	69	2	<1	16	60
	615	5	7	3	84	1	0	14	30
	570[b]	4	0	4	85	7	0	900	8500

[a] Graphite.

[b] Obtained after extended reaction at 570 K.

types of carbon were similar, however, the same sensitivity factor was used for both to estimate surface concentrations.

Tables 1 and 2 and Figs. 1–3 compare surfaces produced after approximately the same number of silicon monolayers reacted (within a factor of 2). Table 2 also includes data for the Cu_3Si–Zn surface after two orders of magnitude more silicon reacted; the silane formation rate was similar (*1*).

The oxygen surface concentration was always less than about 6 at.% after reaction, and in several cases was less than 1 at.% (Tables 1 and 2). Auger spectroscopy is more sensitive to oxygen than to other elements present at the alloy surfaces (except chlorine) (*8*), so the relatively large oxygen peaks in Fig. 1 correspond to low surface concentrations.

The 3-keV, 30-μA beam caused the Cl(180 eV) peak to decrease slightly (up to 20% of its initial value) during recording of the spectra, probably due to electron-induced desorption. The Si(LVV) peak shape did not change significantly, indicating that most of the chlorine that desorbed was not bound to silicon.

Cu_3Si–Zn surface. After reaction on Cu_3Si–Zn at 545 K, prominent AES peaks that indicate silicon bound to chlorine (84 eV) and silicon bound to copper (90 and 94 eV) are clearly resolved (Fig. 3). Bonds between silicon and carbon (90 eV) are also present, since the Si(90 eV)/Si(94 eV) peak amplitude ratio is significantly greater after reaction (Fig. 3). Because of the large effect of electronegativity on peak shift, the Si(94 eV) peak and its companion peak, which contributes to the peak at 90 eV, probably result from silicon bound only to copper (*4*). The additional peak at 90 eV results from silicon bound to carbon, and this silicon may also form bonds to copper but not to chlorine. Similarly, the Si(84 eV) peak is due to silicon which is bound to chlorine, but the silicon may also form bonds to carbon and copper.

Silicon bound to oxygen yields a peak at about 76 eV since oxygen is the most electronegative element present at the alloy surfaces (*4*). Figure 3 has a small peak at 75 eV, indicating that only a small fraction of surface silicon is bound to oxygen. The small peak at 79 eV (Fig. 3) is due to silicon alloyed with copper.

The Si(LVV) spectra recorded after reaction at 585 K (Fig. 2) are similar to those after reaction at 545 K (Fig. 3), but indicate that a larger fraction of surface silicon is bound to carbon, since the Si(90 eV)/Cu(105 eV) and Si(90 eV)/Si(79 eV) peak amplitude ratios are larger and the Si(KVV) spectra are less well resolved, possibly due to the larger 90-eV peak. Thus, the fraction of silicon which is bound to carbon (but not chlorine) appears to increase as reaction proceeds, since more silicon had reacted at 585 K (Table 2).

Although silicon carbide is present at the Cu_3Si–Zn surface after reaction, most of the carbon is graphitic, as indicated by the C(KVV) peak shape (Figs. 2 and 3) (*8, 9*). The large amount of graphitic carbon (Table 2) may cover much of the active surface, which thus may contain more silicon, chlorine, copper, and zinc than indicated in Table 2, especially for the high-carbon-content surfaces.

Cu_3Si surface. The spectra recorded after reaction on Cu_3Si (Figs. 1 and 3) show a broad peak at 90 eV, indicating that a large fraction of the surface silicon is bound to carbon. Furthermore, the C(KVV) peak shape (Fig. 3) is that of silicon carbide and not graphite (*9, 10*). Although no published copper carbide spectra are available for comparison, the copper carbide peak shape would likely differ from that of either silicon carbide or graphite, since other metal carbides (e.g., Ni_3C, TiC, VC, and Cr_3C_2) yield unique C(KVV) peak shapes (*9*). Thus, a significant concentration of Cu—C bonds is probably not present. Although the C(KVV) peak indicates carbidic carbon, a small graphite peak may also be present but masked by the larger carbide peak, since carbon Auger peak shapes of silicon carbide and graphite are similar.

Peak shoulders at 84 and 94 eV indicate the presence of Si—Cl and Si—Cu bonds. The fraction of surface silicon which forms silicon carbide, however, appears larger for Cu_3Si than for Cu_3Si–Zn, since Si(90 eV)/Cu(105 eV) peak amplitude ratios are larger (Figs. 1–3), the Si(LVV) peaks are less well resolved, and the C(KVV) peak shape is that of silicon carbide, not graphite.

The Si(LVV) peak shapes (Figs. 1 and 3) and estimated surface compositions (Table 1) are fairly constant with temperature and extent of reaction. The fraction of surface silicon which forms silicon carbide, however, may increase slightly with increasing extent of reaction; this appears to be the case at 570 K (Fig. 4).

Subsurface composition., Ion bombardment of the Cu_3Si–Zn alloy after reaction of 9×10^4 silicon monolayers indicated that chlorine and carbon were present below the surface. Furthermore, C(KVV) and Cl(180 eV) peak amplitudes decreased at about the same rate with increasing bombardment time. This subsurface region was approximately 500 monolayers thick, as estimated from the ion-bombardment current and an assumed sputtering yield of one (*11*). In contrast, the O(508 eV) peak amplitude decreased rapidly, indicating that little oxygen was present below the surface.

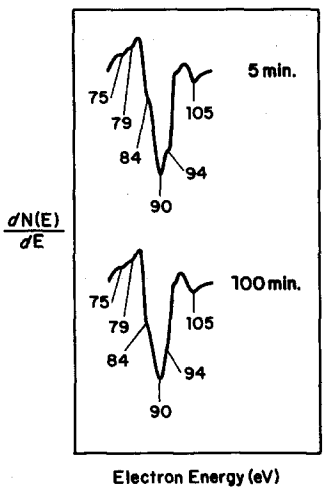

FIG. 4. Si(LVV) and Cu(105 eV) Auger peaks for Cu_3Si after reaction at 570 K for the indicated times. Each spectrum was recorded after reaction on a clean, annealed surface.

TABLE 3

Steady-State Material Balances

Surface	Temperature (K)	CH_3Cl molecules decomposed per silane formed	Nonsilanes formed per decomposed CH_3Cl molecule
Cu_3Si	520	2.5	0.4
	545	3.0	0.2
	570	1.5	0.3
	595	1.5	0.2
Cu_3Si–Zn	545	1.5	0.3
	570	1.5	0.4
	595	1.5	0.3
	615	2.0	0.3

Nonsilane Formation

More CH_3Cl reacted than was incorporated into silanes (Table 3) indicating that some CH_3Cl decomposed. Nonsilane products were detected but not identified, because the GC column did not separate low-boiling nonsilane compounds (e.g., CH_4, H_2, and HCl). Nonsilane product formation rates were estimated, however, using the GC sensitivity for CH_4, a likely product (*3*). Although absolute rates were not determined, these estimates yield useful information about differences between surfaces.

The number of CH_3Cl molecules which decomposed per silane molecule formed and the number of nonsilanes formed per decomposed CH_3Cl molecule were approximately the same for reaction on each alloy (Table 3). For the uncatalyzed reaction on silicon, however, no CH_3Cl decomposition occurred below 670 K (*4*); nonsilanes were formed below 670 K, but these were by-products of the reactions which formed mainly $HSiCl_3$ and CH_3HSiCl_2 (*4*).

DISCUSSION

Clean, Annealed Alloy Surfaces

The surface concentrations of the ion-bombarded alloys (Tables 1 and 2) are

nearly the same as the bulk concentrations. Since the sputtering yields of silicon and copper in copper–silicon alloys are similar (*3*), the surface composition estimates appear to be accurate. The sputtering yield of zinc is larger than that of copper or silicon (*11*), but the zinc bulk concentration in Cu_3Si–Zn is too low to cause the ion-bombarded surface concentrations to deviate significantly from bulk values.

Surface concentration estimates for clean, annealed Cu_3Si (Table 1) indicate that silicon is enriched at the surface to about 30 at.%; this agrees well with results obtained using internal standards and matrix-effect correction factors (*3*).

The clean, annealed Cu_3Si–Zn surface is enriched in silicon and zinc to about 27 and 2 at.%, respectively, apparently because the solid-surface tensions of silicon (1.24 N/m) (*12*) and zinc (0.10 N/m) (*12*) are lower than that of copper (1.67 N/m) (*13*). An impurity (like Zn) segregates to the surface of a binary solid solution provided that the impurity's surface tension is less than that of either main component (*14*). Thus, the surfaces of Cu_3Si and Cu_3Si–Zn appear to behave as solid solutions at 570 K.

Active Sites

The graphitic carbon concentration at the Cu_3Si–Zn surface ranged from about 15 to 85% (Table 2), yet $(CH_3)_2SiCl_2$ selectivity remained high and silane formation rates followed Arrhenius behavior (*1*). Thus, the graphitic carbon did not appear to block active sites for silane formation. It may be that only a small fraction of the surface is active for silane formation. For surfaces after comparable amounts of silicon reaction, the graphite concentration was larger after reaction at higher temperature, indicating that the activation energy for graphite formation is larger than that for silane formation. Surface graphite may form from the carbide, as occurs, for example, on nickel (*15*), and since graphite was only present on the Zn-promoted sample, zinc may increase the rate of conversion of carbide to graphite.

The material balance (Table 3) indicates that CH_3Cl decomposition (to form nonsilanes) occurred simultaneously with silane formation. Kolster *et al.* (*16*) suggested that CH_3Cl decomposition occurs on elemental copper sites formed by depletion of silicon in reacting Cu_3Si. They found that methyl chloride readily decomposed on pure copper (*16, 17*) and between 273 and 473 K formed surface carbon and hydrogen (*17*). Little CH_4 was produced and all the Cl was retained by the surface (*17*). Thus, CH_3Cl may decompose on Cu sites in the alloys to produce carbon, which may preferentially cover the copper (Table 2).

Surface oxygen is also present at the active surfaces, but oxygen does not significantly affect silane formation kinetics since $(CH_3)_2SiCl_2$ selectivity remains high and activity follows Arrhenius dependence even though the oxygen content on Cu_3Si varies from less than 1 up to 6%.

Active sites for selective $(CH_3)_2SiCl_2$ formation apparently contain silicon bound to chlorine, since the active Cu_3Si and Cu_3Si–Zn surfaces contain Si—Cl bonds, and since most silicon at the active surface for the uncatalyzed reaction is bound to chlorine. In addition, HCl and Cl_2 reduce induction times for both uncatalyzed and catalyzed silane formation when added to the CH_3Cl feed or when used to pretreat the solids (*18–22*), apparently by reacting to form Si—Cl surface bonds. Silicon at active sites may also be bound to carbon or copper, since additional silicon bonds to less-electronegative elements do not affect the Si(LVV) peak shift (*4*).

The short induction period for Cu_3Si (*1*) appears to be the time required to form the maximum concentration of active sites containing Si—Cl bonds. The induction period is not due to Cu_3Si formation since Cu_3Si is present initially, nor is it due to increased surface area since no induction period was observed on Cu_3Si–Zn (*1*), indicating that the active surface area was constant.

Role of Copper Catalyst

Alloying copper with silicon reduces induction times by more than two orders of magnitude (*1*). Copper weakens silicon bonds in the alloy (*3*), and this may allow faster reaction between silicon and adsorbed CH_3Cl to form active sites containing Si—Cl bonds. The strong covalent bonding in elemental silicon is modified by alloying with Cu, Au, or Ni (*3, 23, 24*) to form a weaker, more-metallic bonding environment (*3*). This weakened bonding allows faster silicon oxidation; Cu_3Si (*3*), Si(111) covered by gold (*23*), and nickel silicides (*24*) oxidize rapidly at room temperature, yet pure silicon does not (*23*). Thus, metals other than copper (e.g., Zn) may also catalyze Si—Cl bond formation and reduce induction time. Although induction-period rate data are not available for the gold- or nickel-catalyzed reactions, induction times for chromium-, iron-, or tin-catalyzed silane formation (*25, 26*) are less than those for reaction on Si(100) (*4*). This indicates that the active surface for catalyzed silane formation forms faster than does the active surface for the uncatalyzed reaction. The selectivity of the resulting active sites will differ for different catalysts, however, since selectivity depends on additional factors including surface structure and chemical environment.

Methyl chloride apparently dissociates upon adsorption on Cu_3Si to form CH_3 and Cl surface species, since CH_3Cl adsorption forms these species on copper (*17*) and other metals (*17, 27, 28*), and since a Langmuir–Hinshelwood mechanism with dissociative chemisorption models the kinetics (*29*). The CH_3 group decomposes to form hydrogen and graphite or silicon carbide, reacts with hydrogen to form CH_4, recombines to form CH_3Cl, and becomes incorporated into silane products (*1, 18, 19, 30*). Surface Cl species recombine with CH_3 groups to form CH_3Cl, become incorporated into silanes, or diffuse into the bulk. Chlorine species apparently do not combine to form Cl_2, since previous studies have not reported Cl_2 in the product gases (*2, 31, 32*).

The role of the catalyst may be related to its stabilizing or destabilizing influence on adsorbed surface species. Table 4 lists the catalysts for which selectivity data are available, the main products catalyzed by these elements, and catalyst-to-chlorine (M—Cl) bond energies. Data for pure silicon is also included. When catalysts other than copper are used, the selectivity changes significantly. Calcium, which forms a strong ionic bond with chlorine, mainly catalyzes formation of $(CH_3)_3SiCl$. This suggests that the ratio of Cl/Si in the products of the catalyzed reaction will be less than that for the products formed on pure silicon, if the M—Cl bond energy is greater than the Si—Cl bond energy. Such a catalyst can form strong bonds with chlo-

TABLE 4

Silane Formation Catalysts

Catalyst	Main product	Product distribution (mol%)	Secondary product	Product distribution (mol%)	Estimated M—Cl bond energy[a] (kcal/mol)	Selectivity reference
Pb	CH_3HSiCl_2	75	$HSiCl_3$	10	65	25
Cu	$(CH_3)_2SiCl_2$	85	CH_3SiCl_3	10	78	1, 2
Sn	CH_3SiCl_3	85	$SiCl_4$	10	85	25
Fe	CH_3SiCl_3	85	$(CH_3)_2SiCl_2$	10	89	26
Si	$HSiCl_3$	70	CH_3HSiCl_2	20	91	4
Ca	$(CH_3)_3SiCl$	60	$(CH_3)_2SiCl_2$	15	103	26

[a] Ref. (*38*).

rine, reduce the concentration of surface Cl species which participate in silane formation, and thereby reduce the Cl/Si ratio in the silane products. The other catalysts in Table 4 have M—Cl bond energies which are less than or equal to that of Si—Cl, and they catalyze formation of silanes with larger Cl/Si ratios than does calcium.

If the M—Cl bond energy is less than or equal to the Si—Cl energy, other factors must dominate; there is no correlation between M—Cl bond energy and silane Cl/Si ratio for these catalysts (Table 4). Copper may increase the stability of adsorbed CH_3 groups relative to lead, tin, iron, or pure silicon to produce a larger CH_3 group concentration available for participation in the silane formation reaction. This may explain why the C/Cl ratio is larger for silane formation on Cu_3Si alloys than it is for reactions catalyzed by other metals (except calcium) or for reaction on pure silicon.

Of the many mechanisms proposed for direct silane formation (*22, 26, 33–37*), several mechanisms (*26, 33–35*) used electronegativity arguments to assign CH_3 and Cl species to either copper or silicon sites. This approach fails to consider an active surface which contains chlorine and carbide in addition to copper and silicon.

CONCLUSIONS

The surfaces of Cu_3Si and Cu_3Si containing 0.4 at.% zinc promoter were analyzed with Auger spectroscopy after reaction with atmospheric-pressure CH_3Cl.

- Surfaces for selective $(CH_3)_2SiCl_2$ formation contain Si—Cl, Si—Cu, and Si—C bonds after reaction.
- The induction period may be the time required to form the maximum concentration of Si—Cl active sites. Silicon at active sites may also be bound to carbon and copper.
- Copper catalyst may reduce induction time by weakening silicon bonds in the alloy, thus allowing faster formation of active sites containing Si—Cl bonds.
- The Cu_3Si and the zinc-promoted Cu_3Si surfaces differ markedly after reaction. The fraction of surface silicon which formed silicon carbide was smaller for Cu_3Si–Zn than for Cu_3Si; however, the Cu_3Si–Zn surface contained up to 85% graphitic carbon, though no graphite was detected on Cu_3Si.
- Oxygen, present in surface concentrations of up to 6 at.%, does not significantly affect silane-formation kinetics. Only a small fraction of the silicon at the active surface is bound to oxygen.

ACKNOWLEDGMENTS

Support of this work by the National Science Foundation, Grants CPE-8024236 and CPE-8317025, is gratefully acknowledged. We also thank Union Carbide Corporation, Silicones and Urethane Intermediates Division, for partial support of this work. We also appreciate the valuable discussions with Dr. Kenrick M. Lewis.

REFERENCES

1. Frank, T. C., Kester, K. B., and Falconer, J. L., *J. Catal.* **91,** 44 (1985).
2. Voorhoeve, R. J. H., "Organohalosilanes: Precursors to Silicones." Elsevier, Amsterdam, 1967.
3. Frank, T. C., and Falconer, J. L., *Appl. Surf. Sci.* **14,** 359 (1983); Frank, T. C., M.S. thesis. University of Colorado, 1981.
4. Frank, T. C., and Falconer, J. L., *Langmuir* **1,** 104 (1985).
5. Solberg, J. K., *Acta Crystallogr., Sect. A* **34,** 684 (1978).
6. Lewis, K. M., private communication, 1982.
7. Frank, T. C., Ph.D. dissertation, Appendix A. University of Colorado, 1984.
8. Davis, L. E., MacDonald, N. C., Palmberg, P. W., Riach, G. E., and Weber, R. E., "Handbook of Auger Electron Spectroscopy," 2nd ed., Physical Electronics, Eden Prairie, Minn., 1976.
9. Briggs, D., and Seah, M. P., (Eds.), "Practical Surface Analysis by Auger and X-Ray Photoelectron Spectroscopy," Chapter 5. Wiley, Chichester, 1983.
10. Miyoshi, K., and Buckley, D. H., *Appl. Surf. Sci.* **10,** 357 (1982).
11. Coburn, J. W., *J. Vac. Sci. Technol.* **13,** 1037 (1976).
12. Adamson, A. W., "Physical Chemistry of Surfaces," 3rd ed., p. 269. Wiley, New York, 1976.
13. Somorjai, G. A., "Chemistry in Two Dimensions," p. 31. Cornell Univ. Press, Ithaca, New York, 1981.

14. Gupta, R. P., and Perraillon, B., *Surf. Sci.* **103,** 397 (1981).
15. McCarty, J. G., and Madix, R. J., *J. Catal.* **38,** 402 (1975).
16. Kolster, B. H., Vlugter, J. C., and Voorhoeve, R. J. H., *Recl. Trav. Chim.* **83,** 737 (1964).
17. Anderson, J. R., and McConkey, B. H., *J. Catal.* **11,** 54 (1968).
18. Ivanova, N. T., Prigozhina, L. D., Golubstov, S. A., and Gorbunov, A. I., *J. Gen. Chem. USSR* **42,** 1115 (1972).
19. Golubstov, S. A., Ivanova, L. D., Prigozhina, L. D., Andrianov, K. A., Ezerets, M. A., and Fel' dshtein, N. S., *Izv. Akad. Nauk SSSR, Ser. Khim.* **3,** 622 (1972).
20. Turetskaya, R. A., Ivanova, N. T., Andrianov, K. A., Chernyshev, E. A., and Belik, G. I., *J. Gen. Chem. USSR* **46,** 1284 (1976).
21. Lobusevich, N. P., Endovin, Yu. P., and Sporykhina, L. P., *J. Gen. Chem. USSR* **48,** 2264 (1978).
22. Hurd, D. T., and Rochow, E. G., *J. Amer. Chem. Soc.* **67,** 1057 (1945).
23. Cros, A., Derrien, J., and Salvan, F., *Surf. Sci.* **110,** 471 (1981).
24. Valeri, S., Del Pennino, U., and Sassaroli, P., *Surf. Sci.* **134,** L537 (1983).
25. Voorhoeve, R. J. H., and Vlugter, J. C., *Recl. Trav. Chim.* **82,** 605 (1963).
26. Voorhoeve, R. J. H., and Vlugter, J. C., *J. Catal.* **4,** 220 (1965).
27. Anderson, J. R., and McConkey, B. H., *J. Catal.* **9,** 263 (1967).
28. Benziger, J. B., and Madix, R. J., *J. Catal.* **65,** 49 (1980).
29. Voorhoeve, R. J. H., Geertsema, B. J. H., and Vlugter, J. C., *J. Catal.* **4,** 43 (1965).
30. Rochow, E. G., *J. Amer. Chem. Soc.* **67,** 963 (1945).
31. Gorbunov, A. I., Belyi, A. P., and Filippov, G. G., *Russ. Chem. Rev.* **43,** 291 (1974).
32. Launer, P. J., *J. Chem. Eng. Data* **11,** 621 (1966).
33. Keblansky, A. L., and Fikhtengol'ts, V. S., *J. Gen. Chem. USSR* **26,** 2795 (1956).
34. Fikhtengol'ts, V. S., and Keblansky, A. L., *J. Gen. Chem. USSR* **27,** 2535 (1957).
35. Trambouze, P., *Bull. Soc. Chim. Fr.*, 1756 (1956).
36. Podgornyi, I. M., Golubstov, S. A., Andrianov, K. A., and Mangalin, E. G., *J. Gen. Chem. USSR* **44,** 767, 774 (1974).
37. DeCooker, M. G. R. T., Ph.D. dissertation. University of Delft, The Netherlands, 1976; Buechner, N., *in* "Organometallic Chemistry Reviews, 5th International Symposium on Organosilicon Chemistry, August 14–18, 1978" (D. Seyferth, A. G. Davies, E. O. Fischer, J. F. Normant, and O. A. Keutov, Eds.), pp. 409–431. Elsevier, Amsterdam, 1980.
38. Huheey, J. E., *in* "Inorganic Chemistry," 3rd ed., Appendix E. Harper & Row, New York, 1983.